Available online at www.sciencedirect.com
SCIENCE DIRECT®
Journal of Solid State Chemistry 177 (2004) 165–175
JOURNAL OF SOLID STATE CHEMISTRY
http://elsevier.com/locate/jssc

Understanding γ-MnO_2 by molecular modeling

Jörg-R. Hill,[a,*] Clive M. Freeman,[b] and Margaretha H. Rossouw[c]

[a] *Accelrys GmbH, Inselkammerstraße 1, D-82008 Unterhaching, Germany*
[b] *Accelrys Inc., 9685 Scranton Road, San Diego, CA 92121-3752, USA*
[c] *Delta E.M.D. (Pty) Limited, P.O. Box 2197, Nelspruit 1200, Republic of South Africa*

Received 4 March 2003; received in revised form 1 July 2003; accepted 11 July 2003

Abstract

De Wolff disorder, microtwinning, and point defects which are characteristic for γ-MnO_2 have been studied using molecular modeling. Particular attention was paid to the effects these defects have on the X-ray diffraction (XRD) pattern. Comparisons with observed XRD patterns allow identification of structural features in chemical (CMD) and electrochemical (EMD) manganese dioxide. The major factor determining the structure of γ-MnO_2 is de Wolff disorder. CMD materials are characterized by a larger percentage of pyrolusite while EMD materials contain more ramsdellite. Microtwinning occurs to a larger extent in EMD than in CMD materials. EMD materials are also higher in energy.

Keywords: γ-MnO_2; EMD; CMD; de Wolff disorder; Microtwinning; Point defects; X-ray diffraction; Molecular modeling

1. Introduction

Some 200,000 tons of γ-MnO_2 are produced for use in batteries annually. Originally, the term γ-MnO_2 was used collectively to describe a material giving rise to a X-ray powder diffraction pattern (XRD) characterized by poor quality and a number of sharp and broad lines on a diffuse background. Such variability in γ-MnO_2 diffraction profiles indicates that the material is characterized by extended defects in defined crystallographic directions. This view is supported by the fact that the diffraction profile depends to a large degree on the production process used and γ-MnO_2 is therefore labeled as natural (NMD), chemical (CMD), and electrochemical (EMD) manganese dioxide. The broad lines observed in the XRD patterns indicate a high degree of disorder. A number of models have been suggested to account for extended defects in γ-MnO_2 giving rise to the different XRD patterns observed [1]. Extended defects lead to increasingly amorphous materials and it might reasonably be assumed that the XRD patterns for such materials cannot be explained by performing simulations on crystalline structures.

No less than 14 modifications of MnO_2 have been described in the literature [2]. Stoichiometric MnO_2 exhibits three well-characterized polymorphs: ramsdellite [3,4], pyrolusite (β-MnO_2) [5,6], and λ-MnO_2 [7–10]. In idealized close packing arrangements, ramsdellite and pyrolusite possess a common oxygen ion sublattice. The deviations of the real structures from the idealized ones are small (vide infra). They mainly differ in the arrangement of the manganese ions (cf. Fig. 1). γ-MnO_2 is believed to contain parts of ramsdellite and pyrolusite [2] and is characterized by three types of defects: de Wolff disorder—the intergrowth of ramsdellite and pyrolusite [11], microtwinning about the (021) and (061) planes of ramsdellite [2], and point defects such as Mn^{4+} vacancies and Mn^{4+} cations replaced by Mn^{3+} cations [12].

In this paper we show that it is possible to predict the observed XRD patterns of EMD and CMD using systematically constructed models and lattice energy minimizations. Moreover, such simulations also provide insight into the energetics underlying the structural characteristics of EMD and CMD materials. A prerequisite for gaining such an understanding is to test the structural hypotheses available in the literature for validity by performing simulations of the proposed structures and comparisons with experimental information.

*Corresponding author.
E-mail address: jxh@accelrys.com (J.-R. Hill).

0022-4596/$ - see front matter © 2003 Elsevier Inc. All rights reserved.
doi:10.1016/S0022-4596(03)00393-1

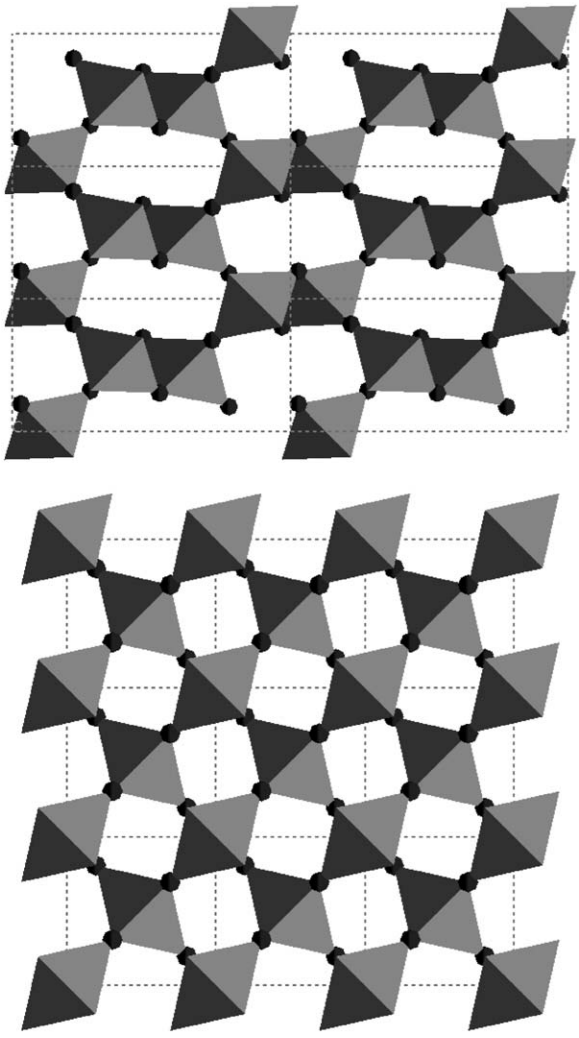

Fig. 1. The structure of ramsdellite (top) and pyrolusite (bottom).

2. Calculations

In order to test structural hypotheses from the literature it is necessary to perform calculations on a number of model systems large enough to correctly reproduce structural features such as defects for EMD and CMD. Since some of the defects described in the literature are extended defects, for example microtwinning [2], the size of the model systems can become large requiring an efficient method of sampling possible structures. This excludes quantum chemical methods which can presently only be applied to the rather small unit cell of manganese dioxide within a reasonable amount of time. Therefore, a force field method is used in the present study.

Metal oxides are accurately modeled using an ion pair potential [13], given availability of a suitably accurate potential model. We note, however, that the choices of an ion pair potential suitable for manganese dioxide are limited. An important initial step in this study is, therefore, centered on the selection and validation of the potential model. We have chosen the augmented consistent valence force field (CVFF) of Vessal [13,14]. The parameters of this force field are shown in Table 1. To test the ability of this force field to reproduce structural features of manganese dioxides, test calculations have been performed for two of its well-characterized modifications, ramsdellite and pyrolusite. For comparison, the structures of these two modifications were also determined using density functional calculations. These calculations were performed using plane waves and the generalized gradient approach (GGA) as implemented in CASTEP [15]. The kinetic energy cutoff for the plane waves was 340 eV, the structure was considered converged when the energy change per atom was less than 2×10^{-5} eV, the root mean square (RMS) displacement less than 10^{-3} Å, and the RMS force less than 5×10^{-2} eV Å^{-1}.

Table 1
Force field parameters of augmented CVFF used in the calculations

	q_i (e)		q_i (e)	
Mn^{4+}	4.0	O	−2.0	
Mn^{3+}	3.0	H	1.0	
		B_{ij} (eV/Å^{12})	C_{ij} (eV/Å^6)	
Mn^{4+}	O	5445.3819	90.465325	
Mn^{3+}	O	2028.0898	0.132531	
O	O	42896.0865	29.351546	
H	O	0.0000	0.000000	
		D_e (eV)	α (Å^{-1})	r_e (Å)
H	O	4.5099	2.28	0.96

Starting from the experimental ramsdellite and pyrolusite unit cells the structures were also determined using the augmented CVFF force field. All force field calculations were performed using GULP [16] employing Ewald sums for the Coulomb interactions. The unit cell was allowed to change in the structure optimizations and the structure was considered to be converged when the gradient norm was less than 10^{-5} eV Å^{-1}. Table 2 shows the results. The augmented CVFF force field is able to predict the unit cells of ramsdellite and pyrolusite with an error of 3% and 2%, respectively. An error of 3% in the ramsdellite unit cell corresponds to an error in the peak positions in the X-ray diffraction pattern (XRD) of about 3% which is sufficient for the purpose of this study.

Once the suitability of the force field had been established models containing the various defects were constructed (vide infra) and their structures optimized using the same convergence criteria as above. The molecular mechanics energies obtained allow estimation of the stability of the different defects.

Table 2
Unit-cell dimensions and root mean square error of ramsdellite and pyrolusite as calculated using the augmented CVFF force field and compared with experiment and DFT calculations

	a (pm)	b (pm)	c (pm)	$\alpha = \beta = \gamma$	RMS (Å)
Ramsdellite, exp. [4]	4.467	9.323	2.850	90.00	
Ramsdellite, calc., DFT[a]	4.467	9.323	2.850	90.00	0.0747
Ramsdellite, calc., CVFF	4.498	9.297	2.931	90.00	0.1369
Pyrolusite, exp. [5,25]	4.414	4.414	2.860	90.00	
Pyrolusite, calc., DFT	4.429	4.429	2.872	90.00	0.0329
Pyrolusite, calc., CVFF	4.403	4.403	2.897	90.00	0.0207

[a]Calculation has been performed at constant volume, therefore the unit cell could not change.

To identify unique structures XRD patterns were calculated employing standard codes (Cerius^2 [17]) and compared. These calculations used the following parameters: wave length 1.54178 Å, unpolarized X rays, no crystal monochromator, Lorentzian peak shape with $u = v = 0$ and $w = 0.06$, and a crystallite size of 100 nm. Background scattering was not considered in the calculations.

The comparison of XRD patterns is a non-trivial undertaking given their highly discontinuous nature. A number of algorithms have been suggested in the literature. We have used the fold algorithm of Karfunkel et al. [18]. This algorithm compares one point of one XRD pattern with the environment of the corresponding point in the other pattern. If $\mathbf{s}_1(i)$ and $\mathbf{s}_2(i)$ with $i = 1, N$ are two XRD patterns of the same resolution defined over the same range of 2θ and normalized to the same value the fold S of the patterns with respect to an $N \times N$ matrix termed fold matrix $\mathbf{F}$ is given by

$$S = (\mathbf{s}_1 - \mathbf{s}_2)\mathbf{F}(\mathbf{s}_1 - \mathbf{s}_2), \quad (1)$$

where the elements of $\mathbf{F}$ are

$$F_{ij} = 1/(1 + \alpha|i - j|^{\beta}). \quad (2)$$

The coefficients $\alpha > 0.0$ and beta are adjustable empirical parameters and have been chosen as $\alpha = 10^{-7}$ and $\beta = 4$ in accord with Karfunkel et al.'s study [18]. The fold S was used as a similarity measure. Small fold numbers imply similarity, zero indicates identical XRD patterns. Comparisons between calculated and observed XRD patterns [19] for EMD and CMD materials were also performed using the same algorithm.

No attempts are made in this study to fit a structure to a given XRD pattern. Therefore, an accurate reproduction of observed XRD patterns cannot be expected. Instead, an XRD pattern is calculated for a given structure and compared with various observed patterns using the algorithm described in the previous paragraph. If the pattern calculated for one structure matches an observed pattern better than the pattern calculated for another structure it is assumed that the first structure is a better model for the system giving rise to the observed pattern than the second structure. A model encompassing the major structural features of γ-MnO_2 can be constructed this way. The match between the calculated and observed patterns could be improved by performing a form of constrained Rietveld refinement. Since the primary interest of this study is to determine which combination of defects can account for observed XRD patterns of γ-MnO_2 this step has not been performed.

3. Models and results

3.1. De Wolff disorder

De Wolff disorder can be described using a layer model. A total of four different layers exists, denoted A, B, C, and D [20]. The coordinates used to construct these layers are summarized in Table 3. Layers B and D might have to be shifted by 1/2 in the c-direction which is indicated by using B′ and D′. Within this model ramsdellite is formed by the sequence …ABCDABCD… while pyrolusite is obtained from …B′DB′DB′DB′D… . Strictly speaking, the atom positions in pyrolusite have slightly different coordinates compared to the ones given in Table 3 ($dx_{Os} = 0.302$, $dx_{Mn} = 0.000$, $dy_{Os} = 0.22$, and $dy_{Mns} = 1.10$), but since these coordinates are only used to construct the starting structure for an optimization we have used the coordinates from Table 3 exclusively. Building a pyrolusite starting structure with one or the other set of coordinates results in the same structure after optimization.

To build de Wolff disordered structures the four different layers (A, B, C, and D) were created and a small program was written which would combine these layers in a given sequence resulting in a trial structure. The unit-cell dimensions were initially set based on the experimental values of ramsdellite, but were allowed to change during the optimization. Therefore, "hinging" of the octahedral chains as described in [21,22] is possible for these structures and different values for the unit-cell dimensions after optimization are possible.

Since the number of possible structures grows exponentially with the number of layers combined it

was decided to build models from a maximum of 24 layers and study every possible combination of layers within this constraint. Considering all allowed possibilities of following one layer with another, a total of 4096 de Wolff disordered structures were built automatically. Since this process could result in identical structures (e.g., the sequence ABCDABCD creates the same structure as the sequence CDABCDAB) unique structures were identified based on their calculated XRD pattern. For these 531 unique structures, geometry optimizations were performed. After the structures had been optimized the XRD patterns were recalculated and compared with observed patterns [19].

Table 4 contains the best matches between calculated and observed XRD patterns. The calculated structures best matching observed XRD patterns from EMD materials (best match for ABCDABD′BCDB′DABCDB′DABCDB′D, 67% ramsdellite, and iba-21, $S = 455.39$, cf. Fig. 2) contained a large proportion of ramsdellite (usually more than 50%) while the best matches for CMD materials (best match for B′DABCDB′DB′DABCDB′DB′DB′DB′DB′D, 33% ramsdellite, and iba-22, $S = 263.88$, cf. Fig. 2) were obtained for structures with a large fraction of pyrolusite. Given the poor match between XRD patterns calculated for all de Wolff disordered structures and observed patterns for γ-MnO_2 it can be concluded that de Wolff disorder alone cannot fully describe the structure of γ-MnO_2.

Table 3
The coordinates of the atoms in the A, B, C, and D layer used to construct the initial structure for the models employed in this study, [20], $a = 4.467$ Å, $b = 9.323$ Å, and $c = 2.85$ Å

Layer	Atom	d_1/a	d_2 (Å)	d_3/c
A	O	$1 - dx_{Ol}$	$-dy_{Ol}$	0
	O	dx_{Ol}	dy_{Ol}	0.5
	Mn	dx_{Mn}	dy_{Mnl}	0
B	O	$0.5 + dx_{Os}$	$-dy_{Os}$	0.5
	O	dx_{Os}	dy_{Os}	0
	Mn	$0.5 + dx_{Mn}$	dy_{Mns}	0.5
C	O	$0.5 + dx_{Ol}$	$-dy_{Ol}$	0
	O	$0.5 - dx_{Ol}$	dy_{Ol}	0.5
	Mn	$0.5 - dx_{Mn}$	dy_{Mnl}	0
D	O	$1 - dx_{Os}$	$-dy_{Os}$	0.5
	O	$0.5 - dx_{Os}$	dy_{Os}	0
	Mn	$-dx_{Mn}$	dy_{Mns}	0.5
Ramsdellite		$dx_{Ol} = 0.211$	$dy_{Ol} = 0.31$	
		$dx_{Os} = 0.333$	$dy_{Os} = 0.23$	
		$dx_{Mn} = 0.022$	$dy_{Mnl} = 1.26$	
			$dy_{Mns} = 1.06$	

The energies calculated for the optimized structures allow a comparison of the relative stability of the de Wolff disordered structures. Pure ramsdellite is 192.5 kJ/mol per formula unit less stable than pure pyrolusite. The calculated energies as a function of the number of pyrolusite layers present is shown in Fig. 3. As can be seen from this figure there is a linear dependence of the relative stability of a structure and the amount of pyrolusite it contains. This can be understood if one considers that the oxygen sublattices of ramsdellite and pyrolusite are nearly identical and that the structures mainly differ in the location of the manganese ions. The energy differences are dominated therefore by differences in the interaction energies between different manganese ions. Since there are closer contacts between manganese ions in ramsdellite this structure must have a higher relative energy and inserting a layer of manganese ions with close contacts results in a constant amount of energy added to the system. Note that the potential model is not wholly electrostatic and energies compared after energy minimization account for lattice relaxation. However, it is apparent that the potential model does not favor ramsdellite inclusion.

Table 4
De Wolff disordered structures whose XRD patterns match best the experimentally observed patterns listed (the naming of the observed XRD patterns follows Ref. [19])

De Wolff disordered structures	Amount of ramsdellite (%)	Quality of match	Matching experimental powder patterns	Type of material
B′DABCDB′DB′DABCDB′DB′DB′DB′DB′D	33	263.88	iba-22	CMD
B′DABD′BCDABCDB′DABCDB′DABCD	67	454.44	iba-40	CMD
ABCDABD′BCDB′DABCDB′DABCDB′D	67	455.39	iba-21	EMD
CDB′DABCDB′DABCDB′DABCDB′DAB	67	496.84	iba-25	EMD
ABCDABD′BCDB′DABCDB′DABCDB′D	67	531.68	iba-23	EMD
CDABCDB′DABCDB′DB′DABCDB′DAB	67	595.78	iba-31	EMD
B′DB′DB′DABD′BCDABCDABCDABCD	67	638.71	iba-15	EMD
B′DB′DABCDB′DABCDB′DABCDABCD	67	668.91	iba-14	EMD
D′BD′BCDB′DABD′BD′BCDB′DABCDAB	50	691.65	iba-12	CMD
B′DB′DB′DB′DB′DB′DB′DB′DB′DB′DB′D	0	855.08	iba-06	β-MnO_2
B′DB′DABD′BD′BCDB′DABCDB′DABCD	50	960.35	iba-08	CMD

The quality of the match is given as value of the fold (cf. text) which would be zero in case of identity, pure ramsdellite has a sequence of ABCDABCD… while pure pyrolusite has a sequence of B′DB′DB′DB′D… .

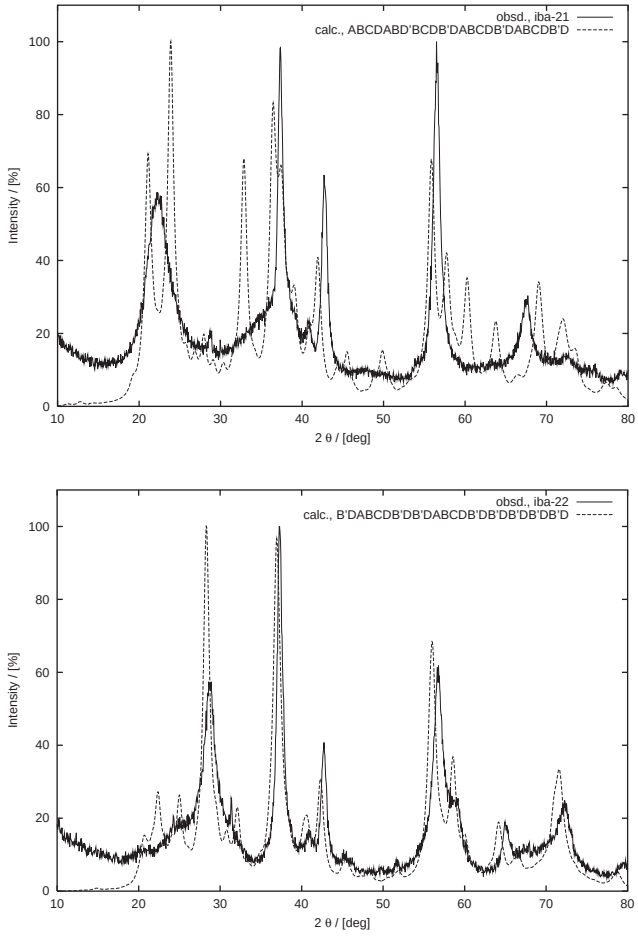

Fig. 2. Comparison of calculated XRD pattern for ABCDABD′BCDB′DABCDB′DABCDB′D with experimental pattern iba-21 (top) and of calculated XRD pattern for B′DABCDB′DB′DABCDB′DB′DB′DB′D with experimental pattern iba-22 (bottom).

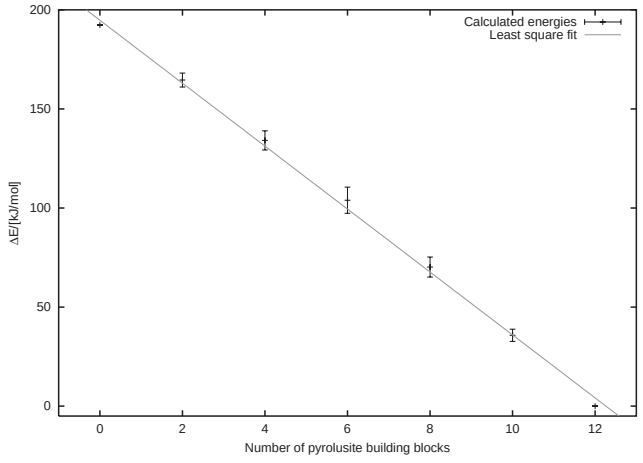

Fig. 3. The calculated energy of de Wolff disordered structures relative to pure pyrolusite, ΔE, as a function of the number of building blocks of pyrolusite, n. The energies can be fitted to a linear equation of the form $\Delta E = -15.878897n + 194.729766$ with a regression coefficient of -99.5%.

3.2. Microtwinning

Microtwinning in manganese oxide can occur about the (021) and (061) planes of ramsdellite [2]. This results in extended defects which can be handled with a periodic model only with rather large systems and under certain assumptions (vide infra).

Structures of microtwinned γ-MnO_2 were generated automatically using a strategy similar to the one described in [2]. Ramsdellite was split along the (021) plane and one of the halves mirrored at the (021) plane. The resulting two halves can be combined again which results in a twinned structure. The twinned structure can formally be considered to be generated by applying two different shifting vectors referred to as R+ and R− in the literature [2]. By applying different sequences of the mirrored and non-mirrored building block (or shifting vectors) it is possible to generate a large number of structures. To create a periodic model it is, however, necessary to apply the same number of R+ and R− shifting vectors in total. Each change in the shifting vector from R+ to R− or vice versa introduces a twin plane in the structure.

We have generated twinned structures automatically by applying all possible combinations of 10 shifting vectors. This resulted in 252 structures (since reading a sequence from left to right and right to left generates the same structure 772 of the 1024 possible structures are either duplicates or not possible due to the need for applying an equal number of R+ and R− shifting vectors). Additionally, structures with only two twin planes were generated, but the distance between these twin planes was systematically increased with n equal shifting vectors being applied ($n = 1 \ldots 16$, 20) before a twin plane was introduced. Unique structures were identified by calculating the XRD patterns for all structures using the same approach as for de Wolff disorder. The resulting 117 unique structures were geometry optimized using the augmented CVFF force field and the XRD patterns were recalculated for the optimized structures.

Comparisons with observed XRD patterns show less similarity for microtwinned structures than for de Wolff disordered structures, but indicate that small numbers of twin planes are preferred in EMD materials (best match for $+++-\ -\ -+++-\ -\ -$, amount of twinning 33%, and iba-19, $S = 1294.49$, cf. Table 5 and Fig. 4). Since the similarity between the XRD patterns calculated for microtwinned structures and observed patterns is even worse than for de Wolff disordered structures, microtwinning alone cannot fully describe the structure of γ-MnO_2.

The calculated energies allow comparison of the stability of the twinned structures with untwinned ramsdellite. The energies obtained in the calculations are lattice energies and not free energies. Nevertheless,

Table 5
Microtwinned structures whose X-ray powder patterns match best the experimentally observed patterns listed

Microtwinned structures	Quality of match	Matching experimental powder patterns	Type of material
+ + + − − − + + + − − −	1294.49	iba-19	EMD
	1309.18	iba-01	EMD
	1319.03	iba-21	EMD
	1356.20	iba-32	EMD
	1361.31	iba-20	EMD
	1402.90	iba-23	EMD
	1478.72	iba-25	EMD
	1508.11	iba-26	EMD
	1552.47	iba-24	EMD
	1587.15	iba-03	EMD
	1756.10	iba-40	CMD
+ − + − + − + − + −	1380.08	iba-06	β-MnO_2
+ + − − − + − + − +	1813.48	iba-22	CMD

The quality of the match is given as value of the fold which would be zero in case of identity.

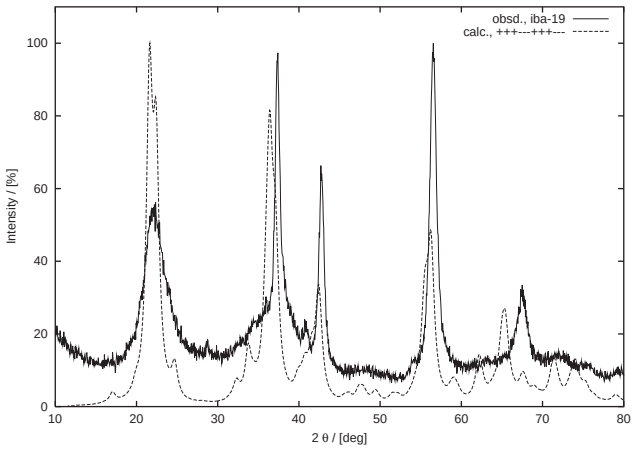

Fig. 4. Comparison of the calculated XRD pattern for twinned structure + + + − − − + + + − − − with experimental pattern iba-19.

they show that the structure with the smallest number of twin planes with the twin planes as far apart as possible is the most stable one. Each twin plane contributes on average 2.4 kJ/mol to the energy of the structure. An increasing density of twin planes also leads to an increase in the calculated density of the structure after optimization. Increasing the distance between two twin planes results in an energy which approaches the energy of the untwinned structure asymptotically. With around nine untwinned blocks between the two twin planes the energy difference becomes smaller than the thermal energy 3/2 RT at room temperature indicating that such structures can be formed at room temperature.

3.3. Point defects

A number of possible point defects for manganese dioxide have been described in the literature [12]. First, there are Mn^{4+} vacancies. The formation of these vacancies can formally be thought of as being described by the following reaction:

$$Mn_xO_{2x} + 4H_2O \rightarrow Mn_{x-1}O_{2x-4}(OH)_4 + Mn(OH)_4. \quad (3)$$

The reaction energy for this reaction can be written as

$$\begin{aligned}\Delta E &= E(Mn_{x-1}O_{2x-4}(OH)_4) - E(Mn_xO_{2x}) \\ &\quad + E(Mn(OH)_4) - 4E(H_2O) \\ &= E(Mn_{x-1}O_{2x-4}(OH)_4) - E(Mn_xO_{2x}) + \text{const.},\end{aligned}$$

$$\Delta\Delta E = E(Mn_{x-1}O_{2x-4}(OH)_4) - E(Mn_xO_{2x}). \quad (4)$$

Second, Mn^{4+} cations can be replaced by Mn^{3+} cations. This defect can formally be described by

$$4Mn_xO_{2x} + 2H_2O \rightarrow 4Mn^{4+}_{x-1}Mn^{3+}O_{2x}H + O_2 \quad (5)$$

which allows calculation of the defect formation energy as

$$\begin{aligned}\Delta E &= 4E(Mn^{4+}_{x-1}Mn^{3+}O_{2x}H) - 4E(Mn_xO_{2x}) \\ &\quad + E(O_2) - 2E(H_2O) \\ &= 4E(Mn^{4+}_{x-1}Mn^{3+}O_{2x}H) - 4E(Mn_xO_{2x}) + \text{const.},\end{aligned}$$

$$\Delta\Delta E = 4E(Mn^{4+}_{x-1}Mn^{3+}O_{2x}H) - 4E(Mn_xO_{2x}). \quad (6)$$

In both cases charge compensation is necessary and it is believed in the literature that this is accomplished by introducing hydrogen atoms making manganese dioxide formally contain water as shown in the reaction equations above [12].

Finally, both types of defects can be combined resulting in the formal reaction

$$\begin{aligned}4Mn_xO_{2x} + 18H_2O \rightarrow\ & 4Mn^{4+}_{x-2}Mn^{3+}O_{2x-5}(OH)_5 \\ & + 4Mn(OH)_4 + O_2 \quad (7)\end{aligned}$$

which allows to calculate the defect formation energy as

$$\begin{aligned}\Delta E &= 4E(Mn^{4+}_{x-2}Mn^{3+}O_{2x-5}(OH)_5) - 4E(Mn_xO_{2x}) \\ &\quad + E(O_2) + 4E(Mn(OH)_4) - 18E(H_2O) \\ &= 4E(Mn^{4+}_{x-2}Mn^{3+}O_{2x-5}(OH)_5) - 4E(Mn_xO_{2x}) \\ &\quad + \text{const.},\end{aligned}$$

$$\Delta\Delta E = 4E(Mn^{4+}_{x-2}Mn^{3+}O_{2x-5}(OH)_5) - 4E(Mn_xO_{2x}). \quad (8)$$

We have studied both types of point defects by either introducing two Mn^{4+} vacancies into a ramsdellite or pyrolusite supercell made out of 24 MnO_2 units ($1 \times 2 \times 3$ unit cells for ramsdellite and $2 \times 2 \times 3$ unit cells for pyrolusite, respectively), by replacing two Mn^{4+} cations with Mn^{3+} cations in a ramsdellite or pyrolusite supercell made out of 32 MnO_2 units ($2 \times 2 \times 2$ unit cells for ramsdellite and $2 \times 2 \times 4$ unit cells for

pyrolusite, respectively) or by introducing one Mn^{4+} vacancy and replacing one Mn^{4+} cation with one Mn^{3+} cation in a ramsdellite or pyrolusite supercell made out of 32 MnO_2 units ($2 \times 2 \times 2$ unit cells for ramsdellite and $2 \times 2 \times 4$ unit cells for pyrolusite, respectively). These defect concentrations are about the same as observed in EMD and are rather high. Therefore, we have chosen the supercell approach in the simulation instead of using a Mott–Littleton defect calculation [23] since the latter predicts defect properties in the dilute limit.

For charge compensation protons were used in the case of Mn^{4+} vacancies which made four of the six oxygen anions surrounding the vacancy OH^- anions. The protons were originally placed 96 pm away from the oxygen ion pointing in the direction of the removed manganese ion. In case of the presence of Mn^{3+} cations one of the surrounding oxygen anions was made an OH^- anion. Due to space constraints the proton had to be placed 96 pm away from the oxygen ion pointing in the direction perpendicular to the Mn–O–Mn plane. The choice of which oxygen anions were made OH^- was random. This approach follows the model by Ruetschi [12]. The chemical composition of the materials studied can be described by the chemical formulae $Mn^{4+}_{0.859}Mn^{3+}_{0.0588}O_{1.613}OH_{0.387}$ or $MnO_{1.97} \cdot 0.179H_2O$. All possible combinations of arranging two defects in the supercell were studied resulting in a total of 70 and 69 structures for ramsdellite and pyrolusite, respectively, in case of Mn^{4+} vacancies and 281 and 496 structures for ramsdellite and pyrolusite, respectively, in case of Mn^{3+} substitutions.

The presence of OH^- ions required the inclusion of a Morse potential for the OH bond since this bond is largely covalent. Where the Morse potential was applied no Coulomb interaction was considered between the oxygen and hydrogen atoms. The force field parameters for the Mn^{3+} ion and the Morse potential are included in Table 1.

The defect energies, ΔE, as defined in Eqs. (4), (6), and (8) cannot be calculated here since calculating the constants defined in these equations requires energies for small molecules such as $Mn(OH)_4$, H_2O, and O_2 which cannot be obtained with the force field used in this study. The force field either does not provide meaningful results for such small molecules or electronic effects such as the reduction of Mn^{4+} to Mn^{3+} cannot be accounted for with a force field at all. Therefore, we can only present $\Delta\Delta E = \Delta E - \text{const.}$ as a measure for the energetical effect of the defect on ramsdellite and pyrolusite and compare these energies only within one type of defect.

Introducing Mn^{4+} vacancies has a different energetical effect on ramsdellite and pyrolusite. $\Delta\Delta E$ is on average -70.2 kJ/mol for ramsdellite and -49.7 kJ/mol for pyrolusite. In contrast, the presence of Mn^{3+} cations has a similar energetical effect on both MnO_2 modifications (41.2 and 50.5 kJ/mol, on average for $\Delta\Delta E$, respectively). Finally, when both types of defects are combined in one model the energetical effect is again different for ramsdellite and pyrolusite. For pyrolusite $\Delta\Delta E$ varies between -4.2 and 110.6 kJ/mol with 92% of the studied systems lower than 20 kJ/mol. For ramsdellite this energy varies between -26.7 and 94.5 kJ/mol with 85% of the studied systems lower than 20 kJ/mol.

Fig. 5 shows the energy of a structure as a function of the distance of two Mn^{4+} vacancies. As can be seen from the figure no simple relationship between the separation of the point defects and the energy can be established. Structures with similar energies can be found for all separations. A similar picture emerges for the other combinations of defects studied here. Therefore, it can be assumed that the distribution of these defects will be random.

The effect of the point defects on the XRD patterns is minimal as can be expected. Table 6 lists the closest matching observed powder diffraction patterns for the 10 best matches found. Not surprisingly, most of the observed powder diffraction patterns are matched by only one ramsdellite structure with Mn^{4+} vacancies. Exceptions are the observed powder pattern iba-06 (pyrolusite) which is matched best by a pyrolusite structure and most of the CMD structures which are best matched by a pyrolusite structure with Mn^{4+} vacancies. Fig. 6 shows the first two entries of Table 6 graphically (iba-22 and iba-32).

Table 7 lists the closest matching observed powder diffraction patterns for the 10 best matches found for a structure with Mn^{4+} cations replaced by Mn^{3+} cations. Most experimentally observed powder diffraction pat-

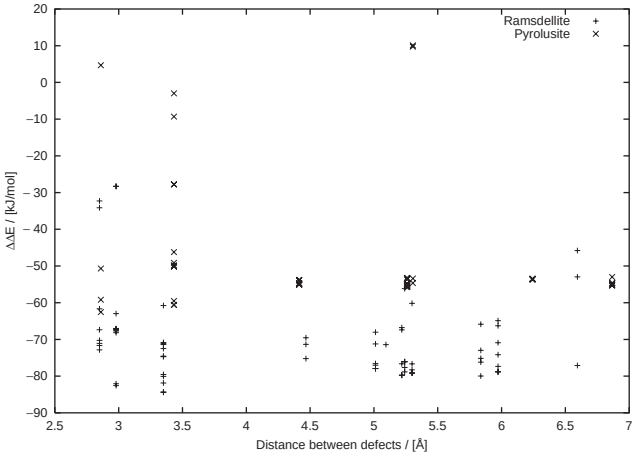

Fig. 5. Energy difference for two Mn^{4+} vacancies, $\Delta\Delta E$, as a function of the distance between the two defects used in the supercell, $\Delta\Delta E$ is defined in Eq. (4), the plots for the other combinations of defects are similar.

Table 6
Structures with Mn^{4+} vacancies whose X-ray powder patterns match best the experimentally observed patterns listed (best 10)

Structure	Distance between defects in Å	Quality of match	Matching experimental powder pattern	Type of material
Pyrolusite	5.260	246.39	iba-22	CMD
Ramsdellite	5.837	667.44	iba-32	EMD
		722.56	iba-21	EMD
		738.51	iba-23	EMD
		770.46	iba-19	EMD
		788.70	iba-20	EMD
		803.46	iba-01	EMD
		829.67	iba-03	EMD
		840.57	iba-15	EMD
		843.36	iba-40	CMD

The quality of the match is given as value of the fold which would be zero in case of identity.

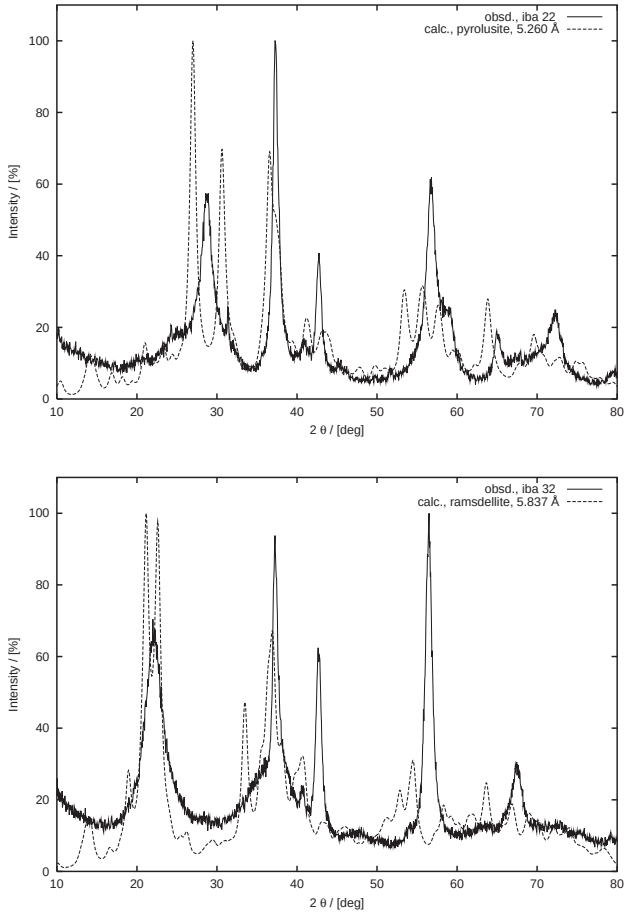

Fig. 6. Comparison of calculated XRD pattern for a pyrolusite structure with Mn^{4+} vacancies with experimental pattern iba-22 (top) and of calculated XRD pattern for a ramsdellite structure with the same defect with experimental pattern iba-32 (bottom).

terns are matched by only a few structures. CMDs are matched best by pyrolusite structures while EMDs are matched best by ramsdellite structures. Fig. 7 shows the

Table 7
Structures with Mn^{4+} cations replaced by Mn^{3+} cations whose X-ray powder patterns match best the experimentally observed patterns listed (best 10)

Structure	Distance between defects in Å	Quality of match	Matching experimental powder patterns	Type of material
Pyrolusite	5.305[a]	606.04	iba-22	CMD
Pyrolusite	5.305[a]	857.55	iba-06	β-MnO_2
Ramsdellite	9.323	1372.45	iba-25	EMD
Ramsdellite	8.092	1166.84	iba-19	EMD
		1171.28	iba-21	EMD
		1177.15	iba-32	EMD
		1190.11	iba-01	EMD
		1216.43	iba-20	EMD
		1238.73	iba-23	EMD
		1354.89	iba-26	EMD

The quality of the match is given as value of the fold which would be zero in case of identity.

[a]Although the distance between the defects in the unrelaxed structure is the same the distribution of the defects is different and the XRD patterns for the relaxed structures differ.

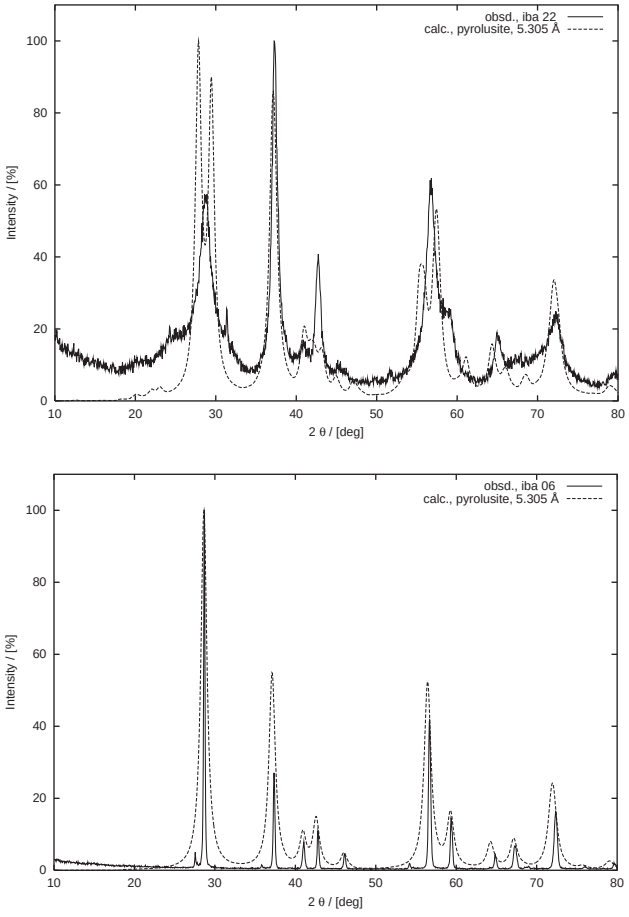

Fig. 7. Comparison of calculated XRD pattern for two different pyrolusite structures with Mn^{4+} cations replaced by Mn^{3+} cations with experimental patterns iba-22 (top) and iba-06 (bottom).

Table 8
Structures with Mn^{4+} vacancies and Mn^{4+} cations replaced by Mn^{3+} cations whose X-ray powder patterns match best the experimentally observed patterns listed (best 10)

Structure	Distance between defects in Å	Quality of match	Matching experimental powder patterns	Type of material
Pyrolusite	3.433	545.11	iba-22	CMD
Ramsdellite	5.972	652.74	iba-21	EMD
		663.25	iba-23	EMD
		682.43	iba-15	EMD
		695.76	iba-40	CMD
		712.98	iba-19	EMD
		726.46	iba-20	EMD
		747.57	iba-03	EMD
		774.26	iba-14	EMD
		786.78	iba-26	EMD

The quality of the match is given as value of the fold which would be zero in case of identity.

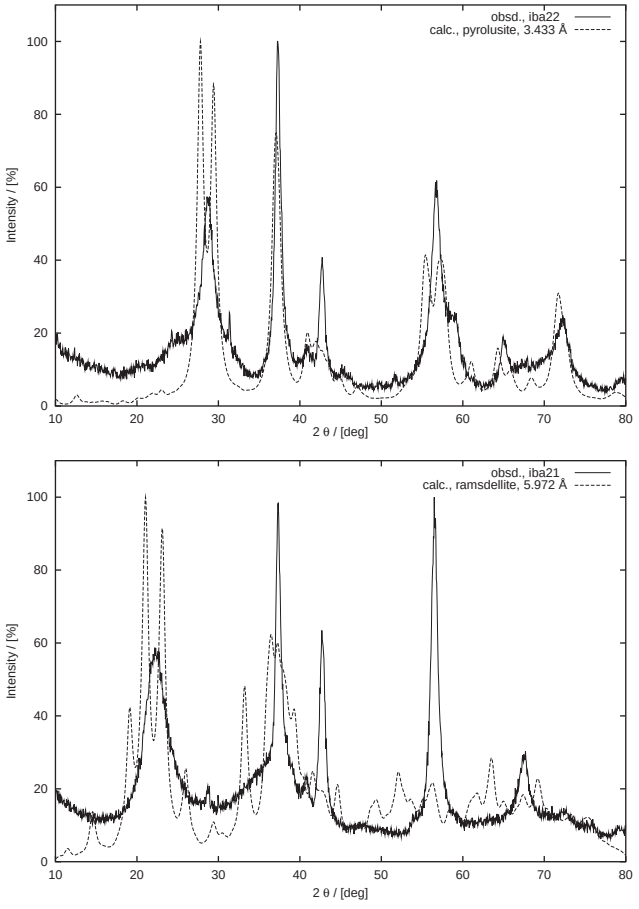

Fig. 8. Comparison of calculated XRD pattern for a pyrolusite structure with a Mn^{4+} vacancy and a Mn^{4+} cation replaced by a Mn^{3+} cation with experimental patterns iba-22 (top) and of a ramsdellite structure with the same defect with experimental pattern iba-21 (bottom).

quality of the matches for the first two structures from Table 7 (iba-22 and iba-06). In general, the quality of the matches is worse than in the case of Mn^{4+} vacancies.

Finally, Table 8 lists the closest matching observed powder diffraction patterns for the 10 best matches found for a structure with one Mn^{4+} vacancy and one Mn^{4+} cation replaced by a Mn^{3+} cation. The best match is obtained for a CMD (iba-22) and a pyrolusite structure. All the other best matches are for one ramsdellite structure and EMDs. Fig. 8 shows the powder diffraction patterns for the first two entries in Table 8 (iba-22 and iba-21). The quality of the matches is comparable with the quality of the matches for two Mn^{4+} vacancies as defects.

However, the similarity between XRD patterns calculated for structures with point defects and observed patterns is small and it might be necessary to combine the different defects to obtain a model which gives rise to an XRD pattern similar to the observed ones for γ-MnO_2.

3.4. Combining all defects

Studying defects separately has shown that de Wolff disorder is the most important defect in explaining the observed XRD pattern, but it alone cannot account for all the features observed. A similar conclusion has been drawn by Schilling and Dahn [20]. We have therefore combined de Wolff disorder and microtwinning in one model. The creation of a microtwinned structure from a de Wolff disordered structure presented a serious challenge. This is due to the fact that the hexagonal lattice of oxygen atoms in the de Wolff disordered structure is slightly distorted which makes it difficult to identify atoms which should be superimposed. The following algorithm was used to build the twinned de Wolff disordered structure.

(1) Take a de Wolff disordered structure and redefine the cell vectors a, b, and c according to the twin plane chosen. This will result in one half of the twin.
(2) Take the cations from step 1 and rotate them by 60°.
(3) Take the anions from step 1 and translate them to fit over the new cation model from step 2.
(4) Merge the new cation and anion models. This will result in the other half of the twin.
(5) Use both halves of the twin in arbitrary order to build stacks of different twins of the de Wolff disordered structure.

We have applied this procedure to one de Wolff disordered structure. We have used the B′DB′DB′DABD′BCDABCDABCDABCD structure which contains 67% ramsdellite and is the best match found for a proprietary MnO_2 produced by Delta EMD. All possible combinations of applying a total of 10 R+ and R− vectors were investigated. Excluding combinations which resulted in the same structure 126 structures have been studied.

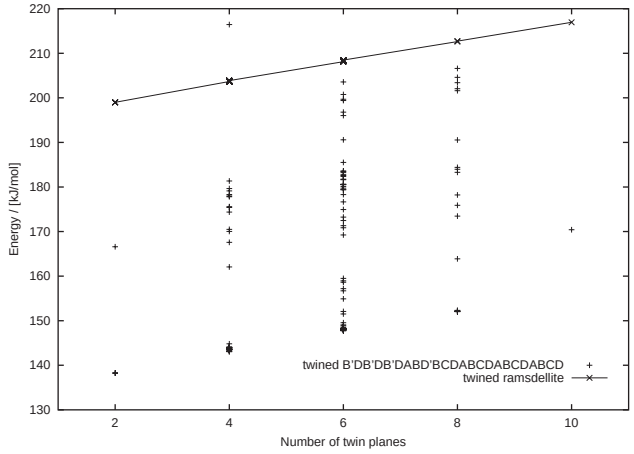

Fig. 9. Energies calculated for the differently twinned de Wolff disordered structure B′DB′DB′DABD′BCDABCDABCDABCD and ramsdellite as a function of the number of twin planes.

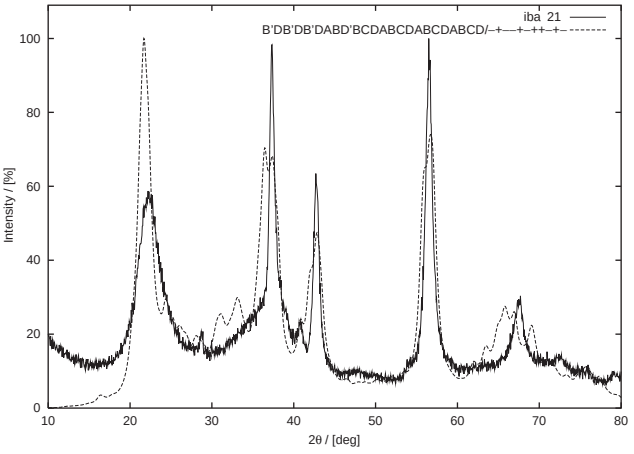

Fig. 10. The XRD pattern calculated for the de Wolff disordered twinned structure shown in inset and compared with the observed XRD pattern for iba-21.

Fig. 9 shows the energies calculated for these structures and compares them with the energies for twinned ramsdellite. While in ramsdellite the energy increases with the amount of twinning this is not the case for the de Wolff disordered structure. For this structure no dependency of the energy from the number of twin planes can be established, for example, structures with two twin planes can differ by as much as 28 kJ/mol.

The XRD pattern calculated for the structure B′DB′DB′DABD′BCDABCDABCDABCD/$-+--+-++-+$ (67% ramsdellite, 80% twinning) which matches best the observed XRD pattern for an EMD material (iba-21) is shown in Fig. 10 ($S = 437.76$). It has a remarkable similarity to the observed XRD pattern which points to the fact that in EMD materials both de Wolff disorder and microtwinning have to be taken into account. The effects of de Wolff disorder and microtwinning on the XRD pattern are, however, not additive (cf. Fig. 11) as assumed in [2].

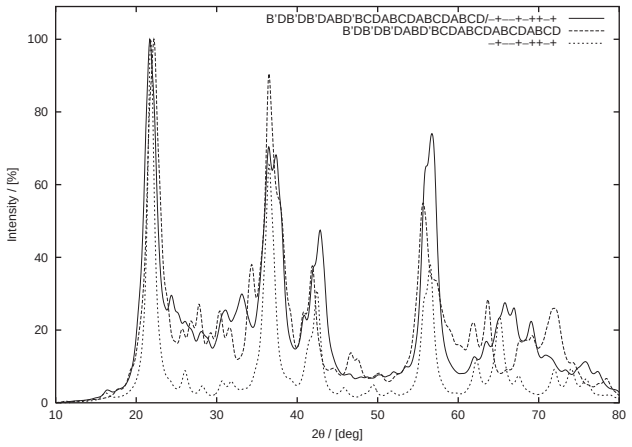

Fig. 11. The XRD pattern calculated for the de Wolff disordered twinned structure shown and compared with the XRD patterns calculated for the de Wolff disordered and the twinned structures shown.

Finally, introducing Mn^{4+} vacancies at random into a de Wolff disordered twinned structure results in a structure with the composition $MnO_{1.968} \cdot 0.214H_2O$ where an improvement in the match with observed powder diffraction patterns is achieved. The similarity with iba-21 improves to 336.18.

4. Summary

The structure and XRD pattern of γ-MnO_2 can be understood by studying the defects playing a role in this system by means of molecular modeling. Studying de Wolff disorder, microtwinning, and point defects separately does not result in XRD patterns with sufficient similarity to the observed patterns. Only when defects are combined a reasonable good match can be obtained.

The major factor determining the structure of γ-MnO_2 is de Wolff disorder. CMD materials (strictly speaking heat treated CMD materials) are characterized by a larger percentage of pyrolusite while EMD materials contain more ramsdellite. This finding contradicts the classification of γ-MnO_2 performed in Ref. [2]. Microtwinning is also important, but occurs more in EMD materials. This explains why Schilling and Dahn's de Wolff disorder based model is able to describe CMD materials well but not EMD materials [20]. Point defects, such as Mn^{4+} vacancies and the replacement of Mn^{4+} cations by Mn^{3+} cations, are also present, but affect the XRD pattern only marginally. The observed XRD patterns of γ-MnO_2 are reasonably, but not fully matched by the ones calculated for a structure containing a combination of different defects. Therefore, it can be assumed that there are either additional defects or

another combination of defects not accounted for in this study playing a role in the structure of γ-MnO_2.

Structural models for MnO_2, of the type illustrated in this paper, form an essential starting point of quantum mechanical calculations. Such calculations would provide the basis for relating electrochemical characteristics to structural understanding. Although, the present work provides the basis for such work, calculations of this type would be very demanding and have not been attempted as yet.

Contrary to common belief it is possible to describe the XRD pattern of γ-MnO_2 by applying crystal tools to a moderately sized supercell. The calculations show that EMD materials are higher in energy than CMD variants owing to the larger proportion of ramsdellite and microtwinning characteristic for them. This supports the view that the formation of EMD materials is kinetically controlled as suggested by Fritsch et al. [24].

Acknowledgments

The authors acknowledge the support of Delta E.M.D. (Pty) Limited and Accelrys Inc. and many valuable conversations with Erich Wimmer during the execution of this work.

References

[1] D.E. Simon, T.N. Andersen, C.D. Elliott, ITE Lett. Batteries New Technol. Med. 1 (2000) 372.
[2] Y. Chabre, J. Pannetier, Prog. Solid State Chem. 23 (1995) 1.
[3] A.M. Byström, Acta Chem. Scand. 3 (1949) 163.
[4] L.D. Konddrasev, A.I. Zaslavskij, Izr. Akad. Nauk SSSR Ser. Fiz. 15 (1951) 179.
[5] J. Brenet, C.R. Acad. Sci. Paris 230 (1950) 1360.
[6] W.H. Baur, Acta Crystallogr. B 32 (1976) 2200.
[7] J.C. Hunter, MnO_2 derived from $LiMn_2O_4$, United States Patent 4,246,253.
[8] J.C. Hunter, J. Solid State Chem. 39 (1981) 142.
[9] J.C. Hunter, MnO_2 derived from $LiMn_2O_4$, United States Patent 4,312,930.
[10] A. Mosbah, A. Verbaere, M. Tournoux, Mater. Res. Bull. 18 (1983) 1375.
[11] P.M. de Wolff, Acta Crystallogr. 12 (1959) 341.
[12] P. Ruetschi, J. Electrochem. Soc. 131 (1984) 2737.
[13] J.-R. Hill, C.M. Freeman, L. Subramanian, Use of Force Fields in Materials Modeling, Vol.16, Wiley-VCH, Wiley, New York, 2000, pp. 141–216.
[14] B. Vessal, in: Catalysis and Sorption Consortium Meeting Minutes, Biosym Technologies Inc., 1994.
[15] Accelrys Inc., Program CASTEP, San Diego, 2001.
[16] J.D. Gale, J. Chem. Soc. Faraday Trans. 93 (1997) 629.
[17] Accelrys Inc., Program CERIUS^2, San Diego, 2001.
[18] H.R. Karfunkel, B. Rohde, F.J.J. Leusen, R.J. Gdanitz, G. Rihs, J. Comput. Chem. 14 (1993) 1125.
[19] D.G. Malpas, F.I. Tye, Handbook of Manganese Dioxides, Battery Grade, IBA Inc. & JEC Press Inc., Brunswick, 1989, (Chapter V).
[20] O. Schilling, J.R. Dahn, J. Appl. Crystallogr. 31 (1998) 396.
[21] L.A.H. MacLean, F.L. Tye, J. Mater. Chem. 7 (1997) 1029.
[22] L.A.H. MacLean, F.L. Tye, J. Mater. Chem. 11 (2001) 891.
[23] N.F. Mott, M.J. Littleton, Trans. Faraday Soc. 34 (1938) 485.
[24] S. Fritsch, J.E. Post, A. Navrotsky, Geochem. Cosmochim. Acta 61 (1997) 2613.
[25] J. Brenet, Bull. Soc. France. Min. 75 (1950) 409.